# Origin of the Conformational Heterogeneity of Cardiolipin-Bound Cytochrome *c*

Yuning Hong,[†] Julia Muenzner,[†] Sebastian K. Grimm,[‡] and Ekaterina V. Pletneva*[,†]

[†]Department of Chemistry and [‡]Thayer School of Engineering, Dartmouth College, Hanover, New Hampshire 03755, United States

S *Supporting Information*

ABSTRACT: Interactions of cytochrome *c* (cyt *c*) with cardiolipin (CL) partially unfold the protein, activating its peroxidase function, a critical event in the execution of apoptosis. However, structural features of the altered protein species in the heterogeneous ensemble are difficult to probe with ensemble averaging. Analyses of the dye-to-heme distance distributions $P(r)$ from time-resolved FRET (TR-FRET) have uncovered two distinct types of CL-bound cyt *c* conformations, extended and compact. We have combined TR-FRET, fluorescence correlation spectroscopy (FCS), and biolayer interferometry to develop a systematic understanding of the functional partitioning between the two conformations. The two subpopulations are in equilibrium with each other, with a submillisecond rate of conformational exchange reflecting the protein folding into a compact non-native state, as well as protein interactions with the lipid surface. Electrostatic interactions with the negatively charged lipid surface that correlate with physiologically relevant changes in CL concentrations strongly affect the kinetics of cyt *c* binding and conformational exchange. A predominantly peripheral binding mechanism, rather than deep protein insertion into the membrane, provides a rationale for the general denaturing effect of the CL surface and the large-scale protein unfolding. These findings closely relate to cyt *c* folding dynamics and suggest a general strategy for extending the time window in monitoring the kinetics of folding.
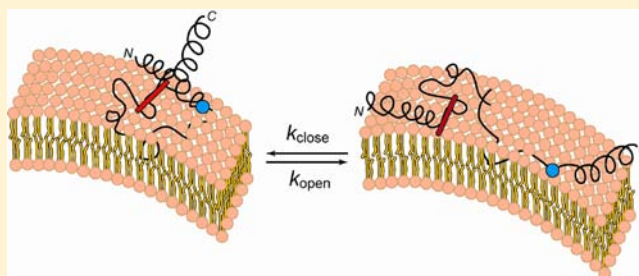
INTRODUCTION

Interactions of proteins with lipid surfaces are essential in biology and have numerous applications in bio- and nano-technology.[1] Protein conformational changes, unfolding, and aggregation are common in these phenomena.[2] Mechanistic details of such transformations, however, remain poorly understood.

Among biological systems, cytochrome *c* (cyt *c*) interactions with cardiolipin (CL)-containing membranes have received considerable attention.[3−5] The binding activates a peroxidase function in cyt *c*, a critical event in early stages of apoptosis, by promoting the protein unfolding.[6,7] Importantly, the peroxidase activity targets CL itself. Peroxidation of CL decreases the strength of cyt *c*−CL interactions, facilitating the protein detachment from the mitochondrial membrane during apoptosis.[5]

Despite many attempts, a consistent structural description of the CL-bound cyt *c* ensemble has been lacking. The protein conformational heterogeneity complicates the analysis of the species with conventional ensemble-averaged probes.[8,9] Recent measurements of time-resolved fluorescence resonance energy transfer (TR-FRET) in dye-labeled cyt *c* revealed distinct populations of surface-bound polypeptide structures, some that are extended and others that are more compact.[10] The protein peroxidase activity paralleled the population of the extended conformers, suggesting a functional link to partitioning between the two types of species. However, the reasons for the coexistence of two types of CL-bound species are not clear nor is it known if they undergo conformational exchange.

Herein we have used a combination of TR-FRET, fluorescence correlation spectroscopy (FCS), and biolayer interferometry (BLI) to develop a systematic understanding of the partitioning between compact and extended cyt *c* conformers and provide information on the dynamics of the bound species. This study has identified factors that influence the types of observed protein species and their interactions with the membrane surface, and offers insights for modulating protein conformational distributions and activity. The findings closely relate to cyt *c* folding dynamics and suggest a general strategy for extending the time window in monitoring the kinetics of folding.

MATERIALS AND METHODS

Preparation of Protein Derivatives. Horse heart cyt *c* mutants Glu92Cys and Glu104Cys were expressed in *Escherichia coli* and purified according to published procedures.[10] Protein labeling with the thiol-reactive reagent bimane iodoacetamide (Invitrogen), 1,5-IAEDANS (Invitrogen), and EZ-Link Maleimide-PEG11-Biotin (Thermo Scientific) and purification of dye-labeled products was done as described.[10] MALDI-TOF mass spectrometry confirmed the labeling. Wild-type cyt *c* isolated from equine heart was purchased from Sigma, reoxidized with an excess of $K_3[Fe(CN)_6]$, and purified

with a fast protein liquid chromatography system (FPLC, GE Healthcare). Heme-free cyt *c* (apocyt *c*) was prepared with the silver sulfate method,[11] the details of which are described in the Supporting Information. Preparation of Zn-substituted cyt *c* (Zncyt *c*) and bimane-labeled Zncyt *c* (ZnBim) is described in the Supporting Information. Protein concentrations were determined by absorbance at 410 nm for heme-containing cyt *c* (ε = 106 100 M^{-1} cm^{-1}),[12] 280 nm for apocyt *c* (ε = 10 900 M^{-1} cm^{-1}),[12] and 423 nm for Zn-substituted cyt *c* (ε = 243 000 M^{-1} cm^{-1}).[13]

Stability Measurements. The unfolding curves of Bim92 cyt *c* in GuHCl were obtained from absorption, CD, and fluorescence measurements (Bim) as previously described.[10] GuHCl concentrations were checked for accuracy with refractive index measurements.

Spectroscopic Measurements. Absorption spectra were measured on an Agilent 8453 diode-array spectrophotometer. Circular dichroism (CD) spectra were recorded with a Jasco J-715 spectropolarimeter. Steady-state fluorescence spectra were recorded on a Horiba Jobin Yvon Fluorolog-3 spectrofluorimeter. The scatter of liposome-containing solutions was removed by subtracting a blank spectrum. Vesicle sizes were determined at room temperature by dynamic light scattering measurement with DynaPro NanoStar (Wyatt Technology Europe GmbH).

Fluorescence lifetimes were measured by time-correlated single photon counting (TCSPC) at 10 000 counts using a NanoLED-375L diode laser (λ_{ex} = 375 nm, <70 ps pulsewidth) as the excitation source and a fast TBX-04 detector. Measurement was done under magic angle conditions. Bim and Dns emission was observed at 480 and 500 nm, respectively.

Data analysis of TR-FRET was done in MATLAB (MathWorks) as previously described.[10] The fluorescence decay rate constant of the unquenched Bim group (k_0) is 10.8 × 10^7 s^{-1} and was determined with the Bim−Cys model compound. The Förster critical distance, R_0, was calculated to be 35 Å for the Bim92 cyt *c* under both native and denatured conditions, according to the method described in the Supporting Information. The value is assumed to be unchanged upon interactions with liposomes, which was validated with heme absorption measurements.

Moment Analysis. The moments (M_n), variance (V), and standard deviations (S) of the $P(r)$ distributions were calculated according to eqs 1 and 2:[8]

$$M_n = \langle r^n \rangle = \frac{\sum P(r) r^n}{\sum P(r)} \tag{1}$$

$$V = S^2 = M_2 - M_1^2 \tag{2}$$

Fluorescence Correlation Spectroscopy (FCS). FCS measurements were performed on a Nikon T*i* Eclipse inverted confocal microscope equipped with a Nikon 60× oil-immersion objective (Plan APO). The microscope was upgraded with compact fluorescence lifetime imaging microscopy (FLIM) and a FCS upgrade kit (PicoQuant, Berlin-Adlershof, Germany). Typically 50 μL of the sample (10−50 nM Bim-labeled protein) was placed on top of a glass coverslip (Corning) and excited with a 405 nm pulsed laser diode (LDH-D-C 405, PicoQuant) controlled by a PDL-800D driver (PicoQuant). The excitation power was approximately 1 mW. The fluorescence emission was passed through a bandpass filter (FF01-482/35, Semrock, Rochester, NY) and focused on a pinhole of 37.9 μm. After the pinhole, the fluorescence emission was probed with a single-photon avalanche photodiode detector (SPAD) and time-correlation data were acquired by PicoHarp 300 (PicoQuant). Measurement and data analysis was performed using SymPhoTime Software (PicoQuant).

In FCS, the autocorrelation function $G(\tau)$ of the fluorescence intensity is given by

$$G(\tau) = \frac{\langle I(t) I(t + \tau) \rangle}{\langle I(t) \rangle^2} \tag{3}$$

where $I(t)$ is the fluorescence intensity at time t, $I(t + \tau)$ is the fluorescence intensity after a time lag τ, and $\langle \rangle$ denotes the time average over the total observation time.

For a single component system associated with the conformational change event (herein, $\mathbf{C} \rightleftarrows \mathbf{E}$), data were fitted to a conformational model with diffusion time τ_D and folding time constant τ_C as described by eq 4:[14,15]

$$G(\tau) = \frac{1}{\langle N \rangle \left[1 + \frac{F}{1-F} \exp\left(-\frac{\tau}{\tau_C}\right) \right] \left\{ \left(1 + \frac{\tau}{\tau_D}\right)\left(1 + \frac{\tau}{\kappa^2 \tau_D}\right)^{0.5} \right\}^{-1}} \tag{4}$$

where $\langle N \rangle$ is the average number of fluorescent molecules in the detection focus, F is the amplitude of τ_C, and κ^2 is the square of the length to the diameter ratio of the focal volume.

Equation 4 assumes that one of the states involving the conformational change event (herein, $\mathbf{C}$) is nonfluorescent and there is no difference in τ_D between the two states. In this case, F corresponds to the average fraction of the molecule in the nonfluorescent state. The model requires the following conditions to be satisfied. First, the rate of the conformational change event should be significantly faster than the diffusion of the molecule, that is, $\tau_C \leq \tau_D$. Second, the fluorescence intensity is significantly different between the two interconverting states.

For FCS measurement, 10 nM labeled protein with 750 μM liposomes were used. Under these conditions, all the labeled protein molecules should be bound to the liposomes. The diffusion time τ_D of CL-bound protein under our experimental conditions was ∼4.0 ms, which allowed observation of the fast conformational dynamic process (sub-ms) between a compact ($\mathbf{C}$, where Bim fluorescence is quenched by heme) and an extended state ($\mathbf{E}$).

The relaxation time constant (τ_C) is expressed according to eq 5:[15]

$$\tau_C = \frac{1}{k_{open} + k_{close}} \tag{5}$$

where k_{open} and k_{close} are the microscopic rate constants of the formation of the $\mathbf{E}$ and $\mathbf{C}$ conformers, respectively. The k_{open} and k_{close} values were obtained from eqs 5 and 6.

$$F = \frac{k_{close}}{k_{open} + k_{close}} \tag{6}$$

The time constant of the Bim triplet state is 3−4 μs, determined with the model Bim−Cys compound, a value consistent with the literature reports.[16] This time constant is much faster than τ_C and τ_D. Similar fits were obtained in tests with and without the triplet component, and the triplet contribution was omitted in later analyses.

Bio-Layer Interferometry (BLI). An Octet Red96 system running in kinetics mode (Pall FortéBio) was used to investigate the kinetics of the cyt *c*−liposome binding interaction. All solutions were dispensed in Greiner Bio-One 96-well polystyrene microplates. The operating temperature was held at 30 °C. After prewetting streptavidin (SA) biosensors (Pall FortéBio) in water for at least 10 min and equilibrating them in buffer (25 mM HEPES buffer at pH 7.4 with 0−150 mM NaCl) for 120 s, biotinylated horse heart cyt *c* Bio104 (2 μM per well) was immobilized to the tips until saturation of the instrument response was reached (480 s). The tips were then washed in a 25 mM HEPES buffer at pH 7.4 with 150 mM NaCl followed by another washing step in buffer. Prior to the vesicle binding step, a first baseline was established by dipping the cyt *c*-covered tips in buffer (300 s). Binding of vesicles to the immobilized cyt *c* was probed at different total lipid concentrations (22−220 μM) and under different ionic strengths for 1200 s. Afterward, the tips were washed again in buffer and a second baseline was established (300 s). No dissociation of vesicles was observed during the washing steps. The biosensors were then incubated with wild-type horse heart cyt *c* (Sigma) at concentrations of 5−20 μM for 2000 s. Dissociation of the wild-type protein was measured for 9000 s after dipping the tips in buffer. For all steps, except the wild-type protein association and dissociation, during

18714

dx.doi.org/10.1021/ja307426k | *J. Am. Chem. Soc.* 2012, 134, 18713−18723
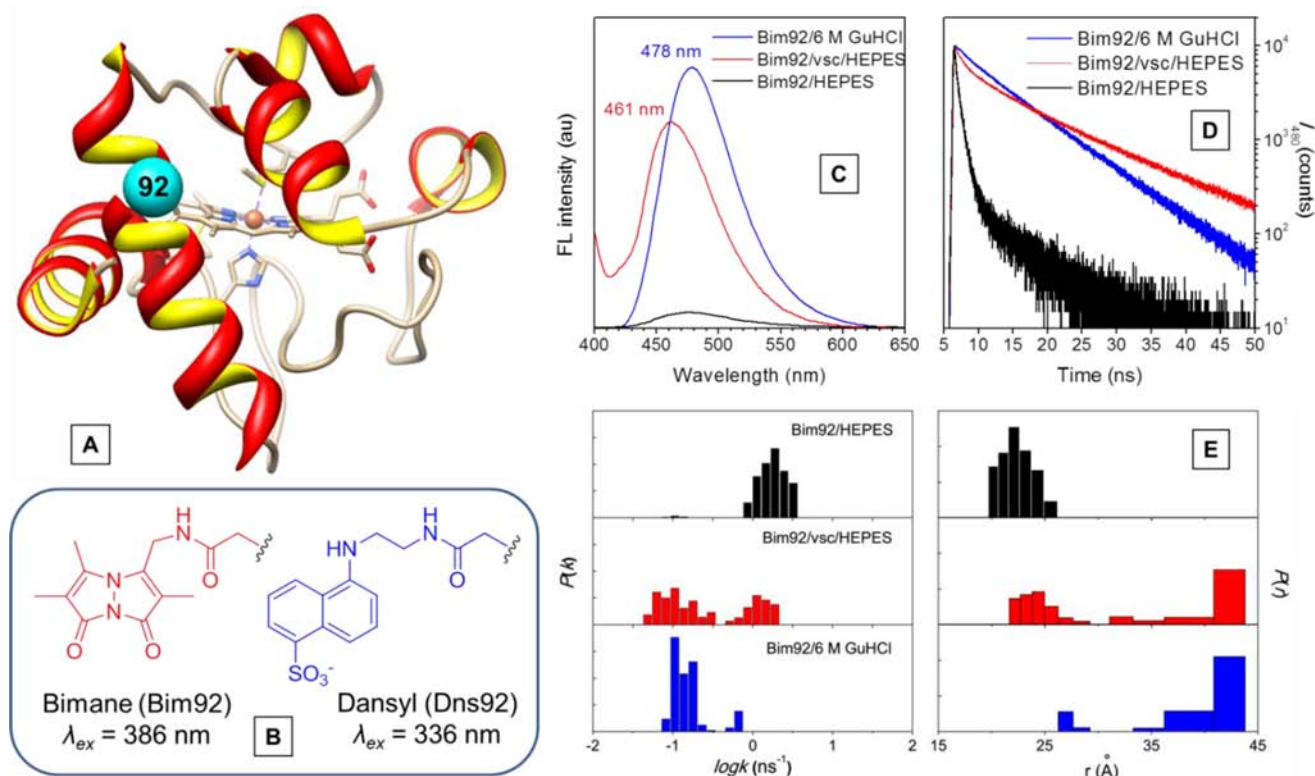
Figure 1. (A) Structure of horse heart cyt c showing the labeled position. (B) Structures of the Bim and Dns labels. (C) Fluorescence spectra (λ_{ex} = 386 nm). (D) TR-FRET decay curves. (E) Distributions of rate constants ($P(k)$, left) and D–A distances ($P(r)$, right) for Bim92 cyt c (0.5 μM) in a 25 mM HEPES buffer at pH 7.4, with TOCL/DOPC (50 mol % CL, 750 μM total lipid) vesicles (vsc) and in 6 M GuHCl solution at pH 7.4. At distances longer than 43 Å, energy transfer rate constants and D–A distances cannot be determined reliably; the structures with $r \geq$ 43 Å are represented by a single bar.

which the plate was agitated at 1000 rpm, the agitation speed was held constant at 600 rpm.

Octet data acquisition and analysis software version 7.0.1 was used to record the data automatically and to align the vesicle binding step and the wild-type association/dissociation steps to their respective baselines. All further analysis was done in MATLAB (Mathworks). For analysis of the vesicle binding to the immobilized cyt c, the raw data were fitted to a monoexponential function yielding the rate constants k_{obs}. Linear regression of k_{obs} on the total lipid concentrations revealed association rate constants k_{on}. Fit to eq 7 of the dependence of the equilibrium wavelength shift R_{eq} on the concentration of the mobile cyt c yielded the apparent association constant K_a.[17] In eq 7, R_{max} is the maximal value of the wavelength shift and [cyt] is the total concentration of the mobile cyt c in solution.

$$R_{eq} = \frac{K_a R_{max}[cyt]}{1 + K_a[cyt]} \tag{7}$$

The dissociation phase was analyzed by fitting the raw data to eq 8, where y is the

$$y(t) = Ae^{-0.01t} + Be^{-k_{off}t} + C \tag{8}$$

wavelength shift, t is the time, k_{off} is the dissociation rate constant, and C is a baseline parameter. The first term was used to model the initial rapid drop of the response signal directly after dipping into a fresh well, and it had a negligible effect on the extracted off-rates. Since no binding of CL-free vesicles to immobilized cyt c was observed during the vesicle association phase and no binding of wild-type cyt c to vesicles could be observed at the highest ionic strength (150 mM NaCl), analysis of the wild-type protein dissociation phase for those traces was omitted.

Laser Photolysis. Kinetics of the ^{3}Zncyt c decay was recorded with transient absorption measurements at 460 nm using a Continuum

Minilite II Q-switched frequency-doubled Nd:YAG laser as an excitation source. The laser delivered 5 ns pulses at 532 nm, and the signal was probed with a 75 W Xe lamp (Oriel, model 66912). A Tektronix DPO 3032 digital phosphor oscilloscope and a ThorLabs DET10A photodiode were adapted to form the detection system. Samples containing 3 μM Zncyt c were prepared in a 25 mM HEPES buffer at pH 7.4 both with and without TOCL/DOPC liposomes (50 mol % CL, 750 μM total lipid). Deoxygenation of the protein samples was carried out by slow bubbling of argon through the solution.

■ RESULTS

Reporters of Cyt c Conformational Heterogeneity. A small fluorophore bimane (Bim) was used to label the Glu92Cys mutant of horse heart cyt c (Figure 1). The labeling site was particularly responsive to the protein interactions with CL liposomes, showing a large blue shift of the dye emission and a high population of extended structures in previous studies with dansyl (Dns) dyes.[10] The red-shifted absorption spectrum of Bim, compared to Dns, and large Stokes shift allowed us to employ visible excitation (405 nm) in our FCS work and minimize problems with scattering from liposome vesicles (Figures S1 and S2 in the Supporting Information). Studies of the Bim-labeled protein not only validate previous findings with another dye, an important objective on its own, but also dramatically increase the information content about cyt c conformational dynamics by enabling a powerful combination of TR-FRET and FCS approaches.

Similar to Dns92 cyt c, the combined effects of Cys mutation and Bim labeling did not alter the cyt c secondary structure and minimally affected the stability of the protein (Table S1 in the Supporting Information). Furthermore, ultracentrifugation

pelleting experiments have revealed that the dye labeling does not change the cyt *c* affinity for CL-containing liposomes (Figure S3, Supporting Information).

Bim fluorescence is quenched in the native folded cyt *c* but greatly increases when the protein is denatured in a 6 M guanidine hydrochloride (GuHCl) solution (Figure 1C). A spectral overlap between the Bim (donor, D) emission and the heme (acceptor, A) absorption spectra suggests FRET as a mechanism of quenching (Figure S1, Supporting Information). Analysis of Bim fluorescence lifetimes in terms of the Förster energy transfer formalism yielded D–A distance distributions $P(r)$ (Figure 1E) similar to that for the Dns-labeled protein (Figure S4, Supporting Information) and consistent with expected distances for the native protein from structural work.[18]

Photoinduced electron transfer (PET) between bimane and Trp has been suggested as an alternative mechanism for the dye quenching.[19] In accord with previous reports,[20] the fluorescence intensity of the Bim model compound became smaller in the presence of Trp, and shorter lifetimes reflected the quenching process (Figure S5A, Supporting Information). The Dns model complex was also affected by the addition of Trp (Figure S5B, Supporting Information); however, the effect was less. The PET phenomenon for Trp–Bim pairs occurs only over relatively short distances and is believed to require a van der Waals contact between the two chromophores.[20] With residues 59 (Trp) and 92 (Bim) separated in the native protein by approximately 14 Å, contact is unlikely. Furthermore, similarities of distance distributions $P(r)$ for Bim92 and Dns92 variants of cyt *c* recovered from the FRET analysis, despite differences in R_0 and PET efficiency (Figure 1E vs Figure S4, Supporting Information) for the two dyes, support FRET as the primary mechanism of quenching. Interestingly, the fluorescence decay curve of the denatured Bim92 variant, where Trp59 and Bim92 can approach each other, differs from that of the model Bim complex, suggesting a possibility of such contact quenching in the denatured protein (Figure 2). However, the small difference in extracted rates (~10%), approaching the resolution limit of the TR-FRET experiments,[10] did not warrant explicit treatment of the PET phenomenon in the subsequent analysis.

Difficulties in the diagnosis of FRET arise from the nonemissive nature of the ferric heme. Substitution of the heme iron with zinc produces a variant, Zncyt *c*, with a fluorescent porphyrin group.[21] Emission of the Zn porphyrin (ZnP) in the native Zncyt *c* increases upon the protein labeling with the Bim group (Figure S6, Supporting Information). Furthermore, upon unfolding of the protein, Bim fluorescence (excited at 386 nm) increases and ZnP emission (excited at 550 nm) decreases as the Bim unit moves away from ZnP. These control experiments further support the conclusion that the mechanism of Bim quenching in folded cyt *c* is FRET to the heme.

Bim fluorescence lifetimes in Bim92 cyt *c* become longer in the presence of CL vesicles (Figure 2). Analysis of the TR-FRET data yielded $P(r)$ distributions with two types of distinct structures, extended (**E**) and compact (**C**) (Figure 1E). These distributions are similar to those found with Dns92 cyt *c*, suggesting that the partitioning into **E** and **C** species is a true feature of the cyt *c* conformational ensemble (Figure S4, Supporting Information).

The relatively long lifetime of Bim fluorescence for the CL-bound extended conformations resembles that seen for the
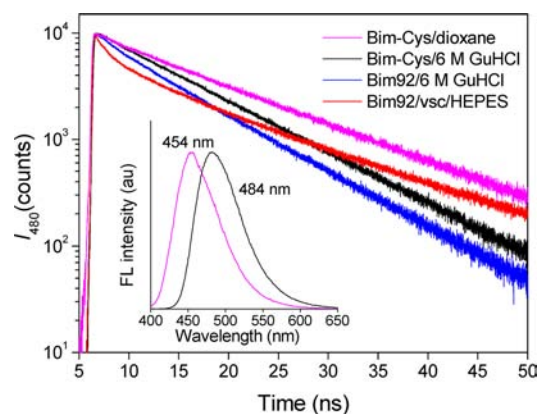

Figure 2. Fluorescence decay curves of the model compound Bim–Cys in dioxane and 6 M GuHCl solution at pH 7.4 and Bim92 cyt *c* (0.5 μM) with TOCL/DOPC (50 mol % CL, 750 μM total lipid) vesicles (vsc) in a 25 mM HEPES buffer and in 6 M GuHCl solution at pH 7.4. The decay curves of Bim–Cys can be fitted to a single exponential function with lifetimes (τ) of 11.80 ± 0.03 and 9.14 ± 0.02 ns in dioxane and in GuHCl, respectively. The decay curves of Bim92 cyt *c* are fitted by a double exponential function, with longer-lived lifetimes (τ_{long}) of 12.03 ± 0.11 and 8.15 ± 0.62 ns with vesicles and in GuHCl solution, respectively. Inset: Normalized fluorescence spectra of Bim–Cys (λ_{ex} = 386 nm) in dioxane and 6 M GuHCl solution. The numbers represent the emission maxima of the spectra.

model Bim–Cys compound in hydrophobic solvents (Figure 2). Binding to CL also introduces a blue shift in Bim92 fluorescence (Figure 1C). The extent of the λ_{max} shift is comparable to that observed for the Dns92 variant but is less than that seen for a model compound in hydrophobic solvents (Figure S7, Supporting Information). In contrast to the GuHCl-denatured protein, with the Bim92 chromophore inserted into the membrane in the **E** species, the group likely will not be accessible for collisional interactions with Trp59.[22]

The decay of the Zncyt *c* triplet state (^{3}Zncyt *c*) is sensitive to the degree of heme exposure.[13] Similar to TR-FRET findings, biexponential kinetics of the ^{3}Zncyt *c* decay (Figure 3) illustrate the heterogeneous nature of the CL-bound protein ensemble, with two types of species that differ in their heme environments. Interestingly, both decay time constants are shorter than that of native Zncyt *c*, suggesting structural
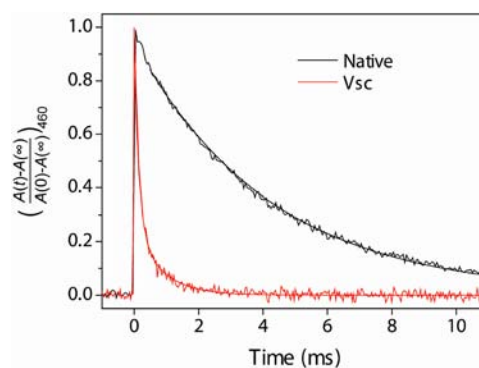
Figure 3. Decay of the triplet ^{3}Zncyt *c* in a 25 mM HEPES buffer at pH 7.4 with (red) and without (black) TOCL/DOPC (50 mol % CL, 750 μM total lipid) vesicles (vsc). The decay of native cyt *c* is monoexponential (τ_1 = 4.24 ± 0.02 ms), and the decay of the CL-bound protein requires fitting to a biexponential function (τ_1 = 0.73 ± 0.04 ms (30%) and τ_2 = 0.13 ± 0.01 ms (70%)).
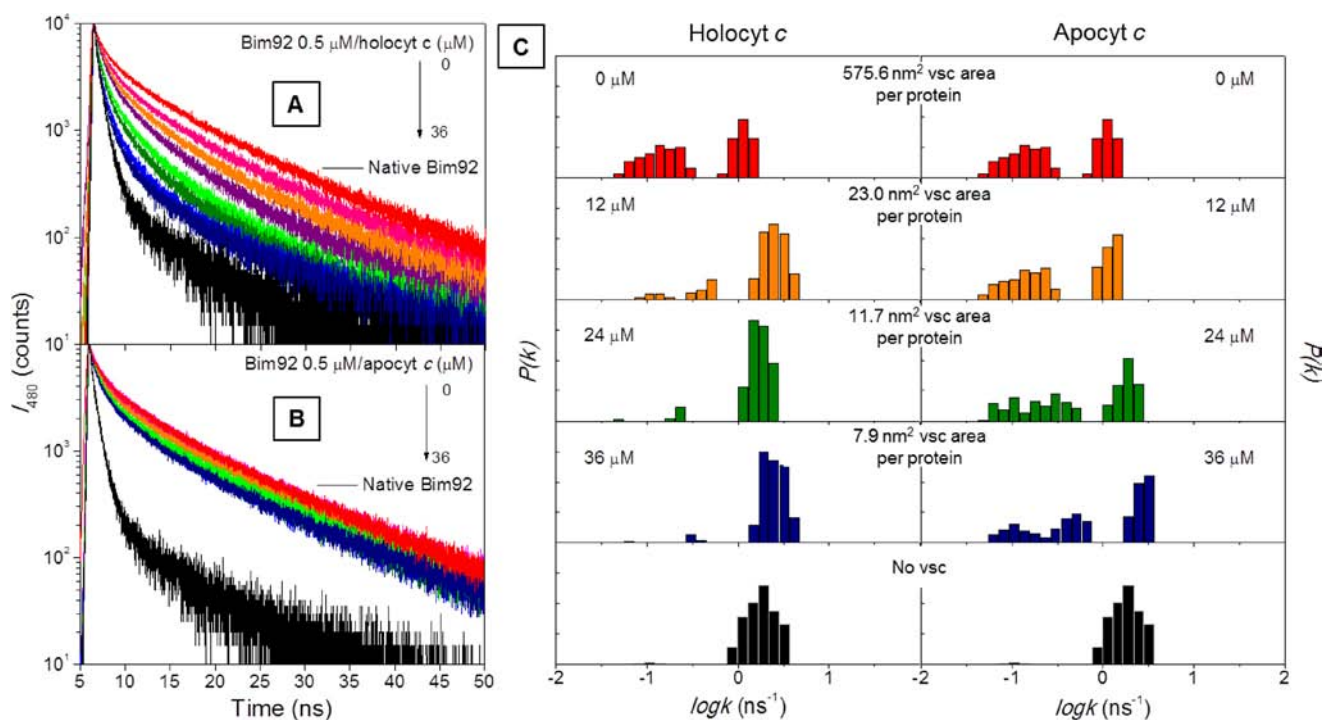
Figure 4. TR-FRET decay curves of Bim92 cyt c (0.5 μM) with TOCL/DOPC (50 mol % CL, 750 μM total lipid) vesicles (vsc) in the presence of different concentrations of (A) holocyt c and (B) apocyt c and (C) the corresponding $P(k)$ distributions. The vesicle surface area that is available per protein is indicated in the panel.

changes in the protein that increase the heme exposure to the solvent in both species.

We wondered whether heterogeneity of the CL-bound ensemble could arise from variability of the vesicles and the higher membrane curvature of small vesicles. All current work focuses on liposomes prepared by extrusion. Compared to vesicles from sonication procedures,[10] these have a more narrow size distribution and are more stable. TR-FRET measurements yielded similar results for Bim92 cyt c bound to CL vesicles of different sizes (Figure S8, Supporting Information), suggesting that the vesicle size is not a factor in the heterogeneous kinetics.

Intermolecular FRET and Effect of Liposome Surface Crowding. Typical FRET experiments in this study involved 40 nm radius vesicles at a total lipid concentration of 750 μM and a protein concentration of 0.5 μM. Assuming a spherical vesicle shape and an average cross-sectional area of the mixed lipid of 0.95 nm^2,[23] the average available membrane surface area per protein is 575 nm^2. These conditions provide plentiful opportunities for cyt c binding and unfolding: generous estimates of the cyt c surface requirements are 9.1 and 74 nm^2 for native and unfolded protein, respectively.[24,25] Although multiple proteins bind to the same liposome, intermolecular fluorescence quenching is unlikely for such low protein surface coverage. Indeed, there is no FRET from Bim to ZnP for the mixture of Bim92 cyt c and Zncyt c (Figure S9, Supporting Information).

Addition of unlabeled holocyt c to the liposome-bound labeled protein shortens the Bim fluorescence decay (Figure 4A). Analysis of the decay kinetics yielded $P(k)$ distributions with an increasingly large fraction of fast rates corresponding to compact structures (Figure 4C). Interestingly, these fast rates are indistinguishable from those of the native protein, suggesting similar Bim-to-heme distances. High protein

concentrations ($\geq$36 μM) lead to partial dissociation of the bound protein (Figure S3, Supporting Information); however, at lower protein concentrations (Figure 4), all cyt c remained bound to CL liposomes. Thus, additional quenching opportunities must arise from short intermolecular Bim–heme distances and the similarities to rates in the native protein suggest tight packing of the globular protein under crowded conditions.

Intermolecular quenching by the heme group is the source of the apparent increase of the compact structures. Vesicle surface crowding with apocyt c does not affect TR-FRET decays (Figure 4B), confirming the assignment of the heme as a quencher and suggesting that there are possibilities for the polypeptide extension on CL liposomes even under crowded conditions on the liposome surface. Reversibility of the CL-induced cyt c unfolding argues against extended species being "stuck" as nonrefoldable conformers.[10,26] Instead, as our results below demonstrate, they participate in the dynamic exchange among the species in the conformational ensemble.

Effect of Ionic Strength. Consistent with the role of electrostatic interactions in cyt c–CL binding,[4,27] ionic strength affects Bim92 fluorescence intensity, position maxima, and corresponding fluorescence decays (Figure 5). The extent of the blue shift decreases, and the population of extended **E** conformers declines with addition of salt. Analysis of the moments of the recovered $P(r)$ distributions (Table 1) indicates that, although the population of the compact conformers increases with higher ionic strength, there is greater variability among these species. The mean Bim–heme distances in the native and CL-bound compact species differ by about 2 Å (Figure 5), and a similar range is seen with the Dns92 variant (Figure S4, Supporting Information). The simultaneous presence of two types of compact species (bound and unbound) could account for the broader $P(r)$ distributions.
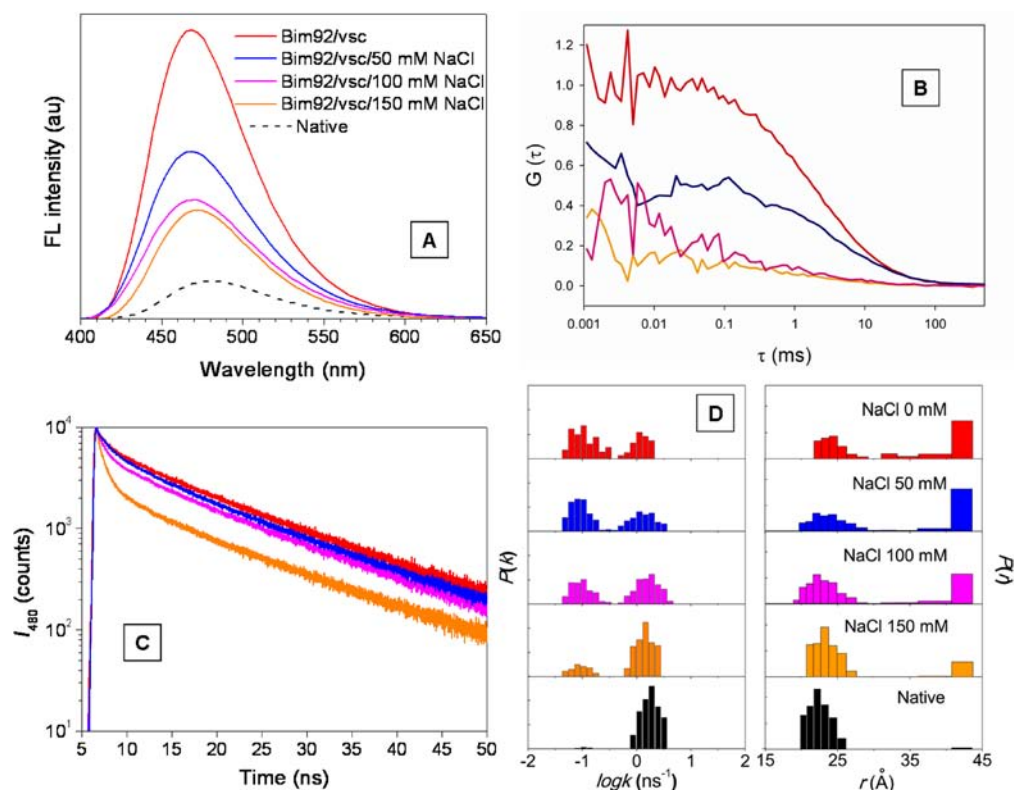
Figure 5. (A) Fluorescence spectra (λ_{ex} = 386 nm), (B) FCS traces, (C) TR-FRET decay curves, and (D) $P(k)$ (left) and $P(r)$ (right) distributions of Bim92 cyt c in HEPES buffer with TOCL/DOPC (50 mol % CL) vesicles (vsc) in the presence of different concentrations of NaCl. $G(\tau)$ is normalized by the average number of molecules in the detection focus ($\langle N \rangle$). Fit residuals with and without an exponential relaxation term are shown in Figure S10B (Supporting Information). Bim92 cyt c in a 25 mM HEPES buffer (pH 7.4) without vesicles is referred to as native Bim92 cyt c. The concentration of Bim92 cyt c was 0.5 μM for steady-state and time-resolved fluorescence experiments and 50 nM for FCS measurement. Total lipid (TOCL/DOPC, 50 mol % CL) concentration was 750 μM for steady-state and time-resolved fluorescence experiments and 75 μM for FCS measurement. At distances longer than 43 Å, energy transfer rate constants and D−A distances cannot be determined reliably; the structures with $r \geq$ 43 Å are represented by a single bar.

Table 1. Analysis of Salt-Dependent Cyt c−Liposome Interactions[a]

Bim92 cyt c	% extended[b]	M_1[c]	V/V_{vsc}[d]	V/V_{nat}[e]
vsc/NaCl 0 mM	62.0	24.2	1.0	1.2
vsc/NaCl 50 mM	47.8	24.1	2.2	2.6
vsc/NaCl 100 mM	42.7	23.1	1.6	1.9
vsc/NaCl 150 mM	19.6	23.4	1.0	1.2
native[f]	1.5	22.5	0.8	1.0

[a]Analysis is based on the TR-FRET results with Bim92 cyt c and TOCL/DOPC vesicles (vsc) (50 mol % CL, 750 μM total lipid, 40 nm radii). [b]Population of extended cyt c structures (log k < −0.5 ns^{-1}). [c]First moment (M_1) calculated from eq 1. [d]Ratio of variance (V) to that of Bim92 cyt c with vesicles in the absence of NaCl. V was calculated from eq 2. [e]Ratio of V to that of the native Bim92 cyt c. [f]Bim92 cyt c in a 25 mM HEPES buffer at pH 7.4.

We have employed FCS to evaluate the possibility of cyt c dissociation from liposomes in the presence of salt. The translational diffusion time of cyt c is approximately 0.15 ms in buffer and is affected little by the protein unfolding.[22] FCS measurements of the GuHCl-denatured Bim92 cyt c yielded 0.2 ms diffusion time, in accord with these reports.[14,22] The slow correlation times of liposome-containing samples varied between 3.8 and 4.5 ms, consistent with the protein binding to a small vesicle.[28] The shapes of the FCS profiles clearly show that cyt c−liposome binding is impaired by salt: slowly diffusing vesicle-bound species contribute progressively less to the

correlation curve (Figure 5B). Quantitative analysis of these curves in terms of the bound protein populations is complicated by Bim quenching, conformational heterogeneity, and binding of multiple fluorescent proteins to a single vesicle. However, even a qualitative decrease in the average correlation time upon addition of salt is a strong indicator of partial dissociation of cyt c from the liposome. The $P(k)$ and $P(r)$ distributions in Figure 5D incorporate these unbound species, and the population of **C** conformers may not be exclusively associated with the CL-bound protein under all solution conditions.

Conformational Dynamics of CL-Bound Cyt c. On the basis of previous analysis of the cyt c−liposome association,[10,17] all the protein is bound to the CL-containing liposomes under our experimental conditions (0.5 μM protein, 750 μM TOCL/ DOPC total lipid, 50 mol % CL, 25 mM HEPES at pH 7.4 with no added salt). In agreement with this conclusion, FCS results at these lipid-to-protein ratios are identical to those at much higher lipid-to-protein ratios of 75 000 to 1 (Figure S10, Supporting Information). The protein is fully bound to CL liposomes, yet adequate fits of the experimental FCS curves require additional components besides a simple diffusional term. Fluorescence intensity fluctuations detected in FCS originate from molecular diffusion but also faster conformational events.[14,15,22] If the two species vary in molecular brightness, their interconversion gives rise to fluctuations in the emitted fluorescence.[14] The **C** and **E** CL-bound species fit this

Table 2. Kinetic Parameters for CL−Cyt c Interactions[a]

entry	samples	τ_C[b] (ms)	F[c]	k_{close}[d] (ms^{-1})	k_{open}[e] (ms^{-1})	k_{on}[f] (M^{-1} s^{-1})
1	10% CL vsc	n.d.[g]	n.d.	n.d.	n.d.	104
2	20% CL vsc	0.14 ± 0.02	0.77 ± 0.02	5.38	1.62	122
3	25% CL vsc	0.16 ± 0.01	0.77 ± 0.01	4.78	1.40	123
4	50% CL vsc	0.58 ± 0.15	0.31 ± 0.03	0.53	1.19	182
5	50% CL vsc/NaCl 50 mM	0.34 ± 0.02	0.43 ± 0.02	1.27	1.67	109
6	50% CL vsc/NaCl 100 mM	0.19 ± 0.01	0.54 ± 0.03	2.79	2.41	75
7	50% CL vsc/NaCl 150 mM	0.13 ± 0.03	0.66 ± 0.03	4.96	2.56	61

[a]Kinetic parameters were obtained from FCS and BLI results. For FCS measurements, Bim92 cyt c and total lipid concentrations were 10 nM and 750 μM, respectively, to ensure proteins are 100%-bound to CL vesicles (vsc). Detailed conditions for BLI experiments are described in Materials and Methods. [b]Relaxation time constant (eq 4) associated with conformational dynamics. [c]Fraction of the proteins in the compact state. [d]Rate constants of the formation of **C** conformers calculated from eqs 5 and 6. [e]Rate constants of the formation of **E** conformers. [f]Association rate constant for liposome binding to immobilized cyt c from BLI. Dissociation rate constant k_{off} remained unchanged (3.0−4.0 × 10^{-4} s^{-1}). [g]Parameters cannot be determined accurately because of the low counts of photons per molecule per second in this sample.
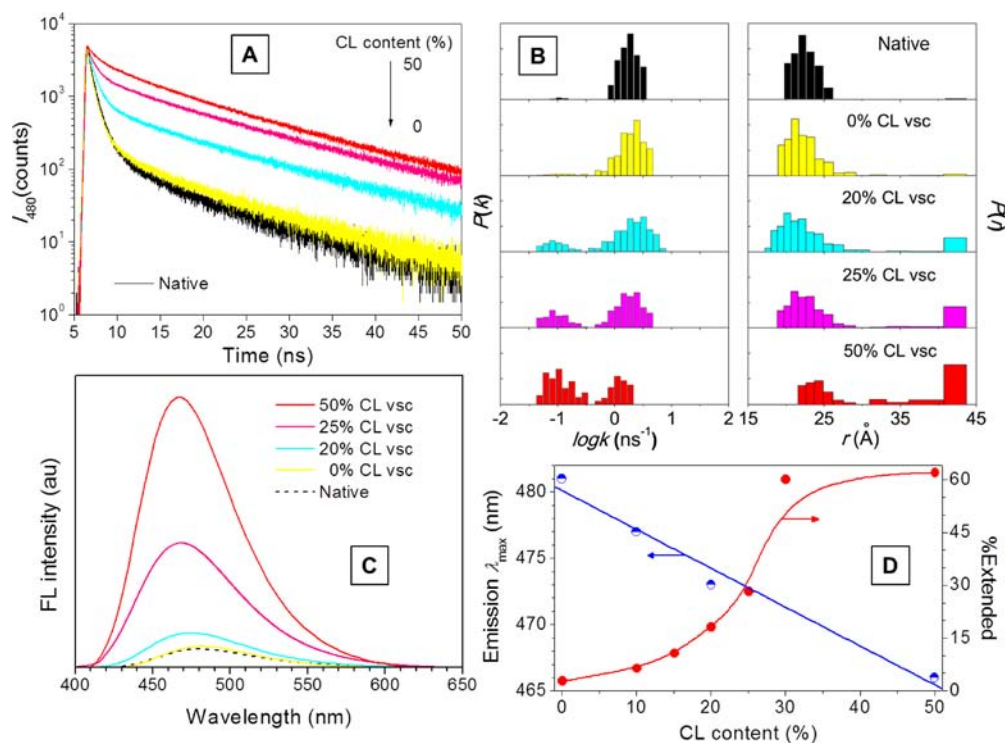
Figure 6. (A) TR-FRET, (B) $P(k)$ (left) and $P(r)$ (right) distributions, and (C) fluorescence spectra of Bim92 cyt c (λ_{ex} = 386 nm) in the presence of TOCL/DOPC vesicles (vsc) with different mol % CL. (D) Change of emission maxima of Bim92 and population of protein conformers with extended structure vs CL content. The lines are shown only to guide the eye. [Bim92 cyt c] = 0.5 μM; [total lipid] = 750 μM. At distances longer than 43 Å, energy transfer rate constants and D−A distances cannot be determined reliably; the structures with $r \geq$ 43 Å are represented by a single bar.

criterion, as they vary greatly in Bim fluorescence intensity because of intramolecular quenching.

Fits with one diffusional component and one exponential relaxation term (eq 4) produced robust values of correlation times for multiple trials with different samples. A time constant of 0.1−0.6 ms (Table 2, entries 4−7, and Figure 5B) reports conformational dynamics associated with changes in Bim quenching (i.e., interconversions between **C** and **E** species). The fraction of molecules undergoing transitions (F, eq 4) is very similar to the fraction of molecules in the compact **C** state from our TR-FRET results (38%, Figure 1E), further supporting that the transitions can be assigned to these dynamics.

Effect of CL Content. Mixtures of zwitterionic DOPC and anionic CL were used to produce liposomes with a range of the

membrane charge densities. The TR-FRET decays and recovered $P(k)$ and $P(r)$ distributions remained unchanged upon mixing with liposomes containing only DOPC (Figure 6A and B), indicating that either there is no binding or cyt c unfolding. Reports suggest that even a small amount of CL (2%) on the membrane surface strengthens cyt c binding to liposomes.[29] Consistent with the improved binding, an increase in the CL mol % shifted the Bim92 emission maximum (Figure 6C). Enrichment of the liposomes with CL also increased the population of the extended **E** conformers.

BLI measurements were employed to determine kinetic parameters k_{on} and k_{off} for cyt c interactions with different liposomes (Figure 7). The method enables measurements of binding interactions on the surface of the fiber optic biosensor and is based on changes in the optical thickness.[30] In contrast
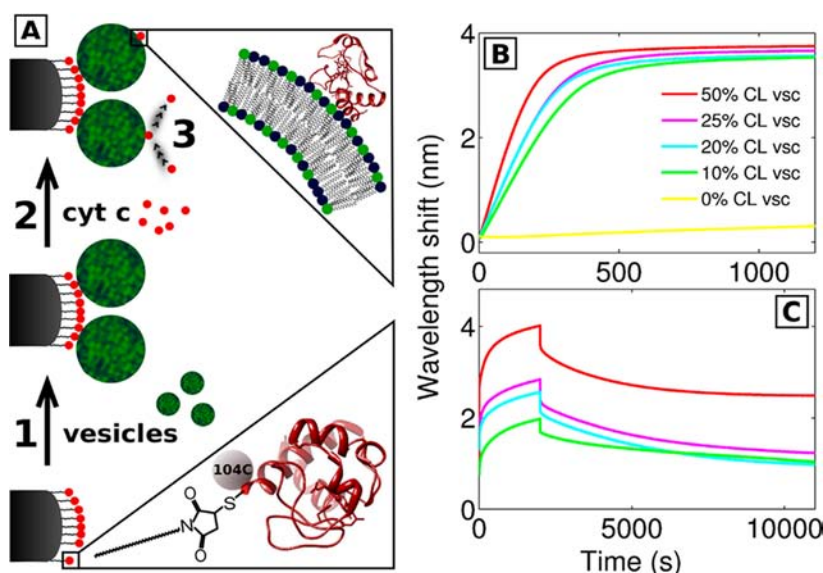
Figure 7. (A) A cartoon illustrating the experimental setup of the biolayer interferometry experiments. Biotinylated cyt *c* Bio104 is immobilized on streptavidin-coated biosensor tips. During the first association phase (step 1), the biosensors are incubated with vesicles until saturation is reached. Afterward, the biosensors are dipped into cyt *c* solutions (step 2) and later on into protein-free buffer so that association and dissociation (step 3) of cyt *c* to vesicles can be examined. (B) Association of vesicles (44 μM) with the indicated CL content to the immobilized cyt *c*. (C) Association (0−2000 s) and dissociation (2000−11 000 s) of label-free cyt *c* (20 μM) from vesicles held at the tip by high-avidity interactions with immobilized Bio104.
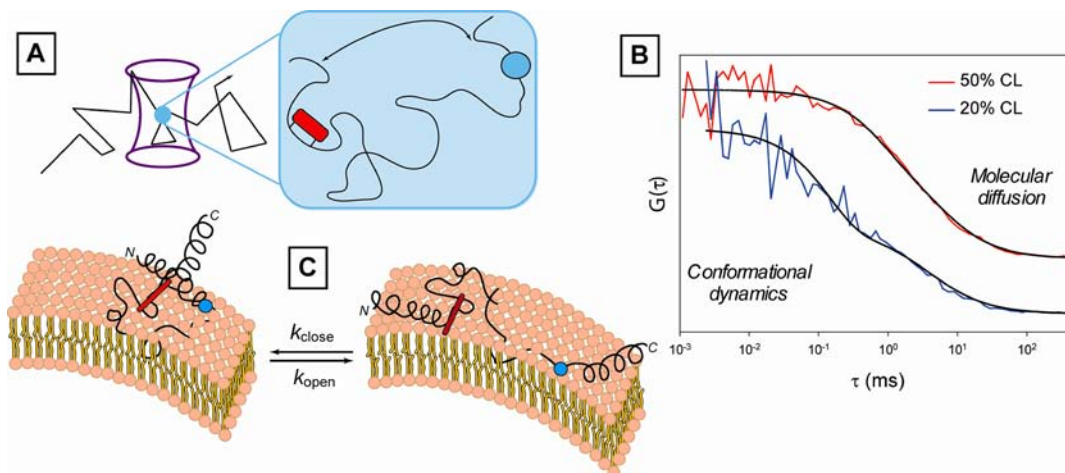
Figure 8. (A) Conformational dynamics revealed by FCS. The heme and Bim92 are shown as a red bar and blue sphere, respectively. (B) FCS traces of Bim92 cyt *c* in a 25 mM HEPES buffer at pH 7.4 with TOCL/DOPC vesicles at 50 and 20 mol % CL. [Bim92 cyt *c*] = 10 nM; [total lipid] = 750 μM. (C) Schematic representation of the conformational exchange of cyt *c* on CL-containing liposome surface.

to many other techniques used to probe cyt *c*−CL interactions, the method does not depend on spectroscopic signatures associated with the cyt *c* unfolding. Biotinylated cyt *c* immobilized on a streptavidin biosensor served to bind and capture liposomes. Dissociation kinetics were probed with mobile cyt *c*. In the experiments with 50 mol % CL, k_{on} values could be determined from both the concentration dependence of k_{obs} for the rates of vesicles binding to the immobilized cyt *c* (Figure 7, step 1) and the analysis of the equilibrium wavelength shift R_{eq} in binding of the mobile cyt *c* to the captured vesicles (Figure 7, step 2, and Figure S11, Supporting Information). Similar values of k_{on} were obtained from both measurements (Table 2 and Figure S11, Supporting Information); these findings enhanced our confidence in the recovered data. Although analysis of the CL−cyt *c* binding within the simplest binding model is likely an oversimplifica-

tion, the observed kinetics are useful markers for comparison of the protein−liposome binding under different experimental conditions. The K_a value of $(3.0 \pm 0.3) \times 10^5$ M^{-1} calculated from the ratio k_{on}/k_{off} at 50 mol % CL agreed well with results from other techniques.[17,31] Dissociation rates (Table 2) were also in accord with previous reports.[4,17]

Weaker binding (at lower mol % CL and with added salt) required a higher concentration of mobile cyt *c* (mM) to reach a saturation signal in R_{eq}. Since high cyt *c* concentrations favor the protein aggregation[32] and cyt *c*−CL interactions depend on the protein coverage of the liposome surfaces,[31,33] we elected to examine instead the binding kinetics at low protein concentration with the immobilized cyt *c*. The strategy provided a robust experimental platform for comparison of binding kinetics within the series of vesicle and solution

conditions. The high lipid-to-protein ratios in this setup more closely resembled conditions of our fluorescence experiments.

As evident from the interferograms (Figure 7B), the CL content strongly affects the kinetics of CL−cyt c interactions. With the increase of CL content, k_{on} values are increased (Table 2, entries 1−4). At 0 mol % CL (DOPC-only liposomes), the interaction is so weak that binding parameters cannot be measured, indicating the importance of the negatively charged CL in binding. An increase in ionic strength with added salt decreases the association rate but has little influence on the dissociation step (Table 2 and Figure S11, Supporting Information). The rate constant k_{off} remained unchanged ((3.0−4.0) × 10^{-4} s^{-1}) in the range of mol % CL and salt concentrations probed.

Measurements of FCS curves at very high lipid-to-protein ratios of 75 000 to 1 revealed that both the amplitude and the rate of the exponential component depend on the CL content (Table 2 and Figure 8B). High concentrations of CL hamper conformational exchange between **C** and **E** species and increase the population of the extended **E** conformers in the cyt c ensemble.

■ DISCUSSION

An increasing body of experimental evidence suggests that cyt c interactions with negatively charged detergents and lipid surfaces lead to partial unfolding of the protein.[6,10,34] The mitochondrial phospholipid CL is particularly effective in promoting cyt c unfolding, and this transformation has dire biological consequences.[35] Cyt c in its altered conformation becomes a potent peroxidase: it catalyzes CL peroxidation, and this activity contributes to release of the protein in apoptosis.[5]

Altered protein conformations, and particularly their heme accessibility, determine the apoptotic peroxidase function of cyt c.[36] However, true structural features of these species in the heterogeneous ensemble are difficult to probe with ensemble averaging. Analyses of TR-FRET measurements and ^{3}Zncyt c decays have revealed two distinct types of CL-bound cyt c conformations, a largely unfolded one, **E**, and another with native-like compactness, **C**.

These conclusions consistently arose from studies of multiple labeled variants and,[10] as this study illustrates, different dyes and labeling approaches. However, observation and analysis of multiple species requires careful choice of experimental conditions. Our findings illustrate that intermolecular quenching may contribute to the fraction of fast decay rates and apparent population of **C** structures (Figure 4). Furthermore, with increased opportunities for quenching, existing **E** structures may become hidden. Intermolecular quenching and unbound protein species may provide deceiving information on the CL-bound ensemble; these aspects have to be considered in the analysis of fluorescence experiments that vary widely in the amount of cyt c that is bound to the liposome surface.

Although intermolecular FRET components can clearly affect TR-FRET data and recovered distributions, they are not playing a role under our typical experimental conditions (0.5 μM protein, 750 μM TOCL/DOPC total lipid). The coexistence of two vastly different types of cyt c conformations, **E** and **C**, is thus a real feature of the CL-bound protein. Our FCS results provide an important piece of mechanistic information about this protein ensemble: the **C** and **E** species are in equilibrium with each other, exchanging on a submillisecond time scale (Table 2). The rate of conformational exchange reflects the protein folding into a compact non-

native state, as well as protein interactions with the lipid surface. Slowed down by interactions with CL, the rate, particularly at higher ionic strength and lower mol % CL, is nevertheless remarkably similar to the one for the formation of the collapsed intermediate during cyt c folding in solution. Time constants between 30 and 60 μs have been reported for conformational fluctuations in the denatured cyt c, and fast folding studies provided estimates of a time constant of ∼55 μs for the formation of the collapsed folding intermediate.[22,37−39]

The compact species likely resembles a molten globular state. The Bim92−heme distances in these conformers, as well as Dns−heme distances in compact species in four other cyt c variants, are very similar in dimensions to that of the native globular protein.[10,40] Previous CD and FTIR studies suggested significant conservation of the protein secondary structure for the CL-bound species.[4,41] The globular α-helical conformation, however, is different from that of the native protein. The lack of the 695 nm charge transfer band argues against native Met80−heme interactions.[6,10] Furthermore, because the rate of the conformational exchange (τ_C) is much faster than the dissociation rate k_{off} (Table 2), there must be continuing interactions that anchor the cyt c polypeptide to the liposome surface.

The nature of the endogenous heme ligand is one of the notable differences between the native and bound compact species. The disruption of the Met80 ligation upon interactions of cyt c with negatively charged lipid surfaces is rapid,[4] yet the progress from the native to the equilibrium CL-unfolded state takes minutes, suggesting that changes in the protein structure extend beyond the heme ligation. On the other hand, the fast rate of the polypeptide opening k_{open} (Table 2) for the lipid-bound conformation indicates that interactions established in the CL-bound **C** structures are transient and likely lack the tight packing seen in the native protein.

The CL surface provides possibilities for both electrostatic and hydrophobic interactions with the bound protein.[42,43] Denaturing conditions of the CL liposome surface destabilize the cyt c native fold and promote the formation of highly extended structures. The break-up of critical stabilizing interactions between the N- and C-terminal helices in the subset of the CL-bound cyt c conformers is one of the important findings of the recent work.[10] In the absence of these contacts, the polypeptide structures are largely open and dominate the peroxidase activity of the protein ensemble. Reestablishment of the contacts between these helices likely drives the conformational exchange between **C** and **E** species. The submillisecond rate of the conformational exchange is consistent with the previously set boundary for this critical refolding step.[38]

Although slower than in solution, the submillisecond rate for the conformational exchange of CL-bound protein points to the ease of the polypeptide closure of the lipid-interacting cyt c, suggesting that the majority of the polypeptide likely resides on the liposome surface. The predominantly peripheral binding, rather than deep protein insertion into the membrane, is in agreement with previous results.[10,44] Our fluorescence findings do not provide any indication of the previously suggested CL acyl insertion into the cyt c interior,[45] a result related to the experimental methods and perhaps also to the choice of the experimental conditions. Interestingly, the extended conformations of the CL-bound cyt c are not much different in their degree of unfolding from the ones induced by acid and GuHCl denaturation.[40] In solution, unfolding truly proceeds in three

dimensions and the similarities of the surface and solution-denatured species further support the dynamic nature of the CL-bound protein.

Electrostatic attraction between cationic cyt c and the anionic CL liposome surface drives the protein−lipid binding.[4,10,46,47] The importance of electrostatic forces is particularly apparent from the absence of cyt c binding to the neutral CL-free liposomes. The protein−liposome interactions are noticeably weaker in the presence of salt, with k_{on} decreasing upon addition of salt that screens the surface charges.

The k_{off}, however, remains constant within the studied range of ionic strengths and CL concentrations, suggesting also the role of nonelectrostatic forces in the established CL−cyt c interactions. The slow rate of cyt c dissociation is consistent with some entrapment of the cyt c by the lipid. Both the N- and C-terminal helices of cyt c have been implicated in interactions with the CL membranes, and the polypeptide fragment in the vicinity of residue 92 appears to partially insert into the bilayer.[10,24,42,46] The long lifetime and blue shift of the Bim92 chromophore in the studied cyt c variant suggest that this group does enter the hydrophobic environment of the membrane. Partial polypeptide insertion into the membrane near residue 92 could provide protein anchoring yet still allow for the conformational interconversions that bring the heme and the Bim92 label close, particularly if the N-terminal helix can swing between open and closed conformers.

The kinetics of conformational exchange depend on the CL content of the membrane (Table 2), suggesting that the polypeptide interactions with CL influence the formation of the non-native compact species. Under conditions approaching the typical CL content of the inner mitochondria of mammalian cells (10−20%),[48] cyt c interconversions significantly accelerate and the population of the E species declines (Figure 8C and Table 2). Although under these conditions the E species may not be as prominent and their effects may not be as impressive as in vitro studies, the peroxidase activity of the CL-unfolded cyt c has sound biological significance,[5,7,10] with strong support from in vivo results.[5] Furthermore, redistribution of CL, an important functional process during early stages of apoptosis, could influence the cyt c conformational interconversions and thus associated peroxidase activity.[49]

Cyt c has been a true workhorse for studies of protein folding, with experimental results and insights guiding the field.[25,50,51] Although not easy to probe, populations of C and E conformers have been observed in the denatured protein and the importance of the compact intermediates, as well as the C ⇌ E conformational exchange during folding, has emerged from recent work.[8,37,52] Alterations of the cyt c structure by CL show intriguing similarities to the protein folding mechanism in solution. Not only can the types of structures be explained using folding subunits,[10,51,53] the ensemble heterogeneity and the C ⇌ E conformational exchange are also important features of the lipid-bound species with implications for functional activity.

Studies of the liposome-bound cyt c suggest a convenient strategy for investigations of protein folding dynamics. The C ⇌ E conformational exchange is associated with a critical compaction step in protein folding, yet its submillisecond time scale is particularly challenging for experimental observation. The time scale of these dynamics overlaps with the time scale of molecular diffusion for many proteins popular in folding research. As our results with cyt c show, the latter can be slowed down by binding or tethering to slowly diffusing particles, allowing slow conformational processes to be monitored by FCS.

■ CONCLUSIONS

Analyses of the CL-bound cyt c with multiple kinetic probes have consistently revealed two distinct types of bound protein conformations. The two structures are not independent but undergo conformational exchange related to the break-up and reestablishment of contacts between the protein's N- and C-terminal helices. Electrostatic interactions with the negatively charged lipid surface, including changes in CL concentrations, strongly affect the kinetics of cyt c binding and conformational exchange. The predominantly peripheral binding mechanism, rather than deep protein insertion into the membrane, explains the general denaturing effect of the CL surface and the large-scale protein unfolding.

The C ⇌ E conformational dynamics directly affect the population of the largely unfolded cyt c structures and, therefore, the protein peroxidase activity. The existence of exchange between the two types of bound species implies the possibility of population shifts and suggests a pathway to altering the apoptotic peroxidase activity through the C conformers. For exchanging C and E species, dissociation of C from the liposome surface by a competitive binder will also change the amount of E conformers. Regulators that target better defined C conformers are easier to rationally design than ones for the elusive E species.

■ ASSOCIATED CONTENT

ⓈSupporting Information
Additional Materials and Methods; Bim-heme spectral overlap; Bim−Cys fluorescence; ultracentrifugation binding assay; $P(\hat{k})$ and $P(r)$ distribution of Dns92 cyt c; model compounds quenching by Trp; emission spectra of Bim-labeled Zncyt c; Dns92 fluorescence decay curves; effect of vesicle size on CL-bound cyt c; fluorescence of the mixture of Bim92 cyt c and Zncyt c; autocorrelation curve of Bim92 cyt c with CL vesicles; binding kinetics of mobile cyt c to captured vesicles; interferograms of vesicle binding and cyt c dissociation; table of thermodynamic parameters of cyt c unfolding. This material is available free of charge via the Internet at http://pubs.acs.org.

■ AUTHOR INFORMATION

Corresponding Author
ekaterina.pletneva@dartmouth.edu
Notes
The authors declare no competing financial interest.

■ ACKNOWLEDGMENTS

■ REFERENCES

(1) Gray, J. J. Curr. Opin. Struct. Biol. 2004, 14, 110−115.
(2) Shin, I.; Kreimer, D.; Silman, I.; Weiner, L. Proc. Natl. Acad. Sci. U.S.A. 1997, 94, 2848−2852. Al Kayal, T.; Nappini, S.; Russo, E.; Berti, D.; Bucciantini, M.; Stefani, M.; Baglioni, P. Soft Matter 2012, 8, 4524−4534. Endo, T.; Eilers, M.; Schatz, G. J. Biol. Chem. 1989, 264, 2951−2956.

(3) Iverson, S. L.; Orrenius, S. *Arch. Biochem. Biophys.* **2004**, *423*, 37−46. Beales, P. A.; Bergstrom, C. L.; Geerts, N.; Groves, J. T.; Vanderlick, T. K. *Langmuir* **2011**, *27*, 6107−6115.

(4) Sinibaldi, F.; Fiorucci, L.; Patriarca, A.; Lauceri, R.; Ferri, T.; Coletta, M.; Santucci, R. *Biochemistry* **2008**, *47*, 6928−6935.

(5) Kagan, V. E.; Tyurin, V. A.; Jiang, J.; Tyurina, Y. Y.; Ritov, V. B.; Amoscato, A. A.; Osipov, A. N.; Belikova, N. A.; Kapralov, A. A.; Kini, V.; Vlasova, I. I.; Zhao, Q.; Zou, M.; Di, P.; Svistunenko, D. A.; Kurnikov, I. V.; Borisenko, G. G. *Nat. Chem. Biol.* **2005**, *1*, 223−232.

(6) Kapralov, A. A.; Kurnikov, I. V.; Vlasova, I. I.; Belikova, N. A.; Tyurin, V. A.; Basova, L. V.; Zhao, Q.; Tyurina, Y. Y.; Jiang, J.; Bayir, H.; Vladimirov, Y. A.; Kagan, V. E. *Biochemistry* **2007**, *46*, 14232−14244.

(7) Hüttemann, M.; Pecina, P.; Rainbolt, M.; Sanderson, T. H.; Kagan, V. E.; Samavati, L.; Doan, J. W.; Lee, I. *Mitochondrion* **2011**, *11*, 369−381.

(8) Pletneva, E. V.; Gray, H. B.; Winkler, J. R. *Proc. Natl. Acad. Sci. U.S.A.* **2005**, *102*, 18397−18402.

(9) Perroud, T. D.; Bokoch, M. P.; Zare, R. N. *Proc. Natl. Acad. Sci. U.S.A.* **2005**, *102*, 17570−17575. Haas, E. *ChemPhysChem* **2005**, *6*, 858−870.

(10) Hanske, J.; Toffey, J. R.; Morenz, A. M.; Bonilla, A. J.; Schiavoni, K. H.; Pletneva, E. V. *Proc. Natl. Acad. Sci. U.S.A.* **2012**, *109*, 125−130.

(11) Fisher, W. R.; Taniuchi, H.; Anfinsen, C. B. *J. Biol. Chem.* **1973**, *248*, 3188−3195.

(12) Stellwagen, E.; Rysavy, R.; Babul, G. *J. Biol. Chem.* **1972**, *247*, 8074−8077.

(13) Tremain, S. M.; Kostic, N. M. *Inorg. Chem.* **2002**, *41*, 3291−3301.

(14) Haldar, S.; Mitra, S.; Chattopadhyay, K. *J. Biol. Chem.* **2010**, *285*, 25314−25323.

(15) Neuweiler, H.; Johnson, C. M.; Fersht, A. R. *Proc. Natl. Acad. Sci. U.S.A.* **2009**, *106*, 18569−18574.

(16) Kosower, E. M.; Giniger, R. *J. Phys. Chem.* **1988**, *92*, 1140−1142.

(17) Stepanov, G.; Gnedenko, O.; Mol'nar, A.; Ivanov, A.; Vladimirov, Y.; Osipov, A. *FEBS Lett.* **2009**, *583*, 97−100.

(18) Bushnell, G. W.; Louie, G. V.; Brayer, G. D. *J. Mol. Biol.* **1990**, *214*, 585−595.

(19) Mansoor, S. E.; Dewitt, M. A.; Farrens, D. L. *Biochemistry* **2010**, *49*, 9722−9731.

(20) Mansoor, S. E.; McHaourab, H. S.; Farrens, D. L. *Biochemistry* **2002**, *41*, 2475−2484.

(21) Ensign, A. A.; Jo, I.; Yildirim, I.; Krauss, T. D.; Bren, K. L. *Proc. Natl. Acad. Sci. U.S.A.* **2008**, *105*, 10779−10784. Lee, A. J.; Ensign, A. A.; Krauss, T. D.; Bren, K. L. *J. Am. Chem. Soc.* **2010**, *132*, 1752−1753.

(22) Choi, J.; Kim, S.; Tachikawa, T.; Fujitsuka, M.; Majima, T. *Phys. Chem. Chem. Phys.* **2011**, *13*, 5651−5658.

(23) Pinheiro, T. J.; Cheng, H.; Seeholzer, S. H.; Roder, H. *J. Mol. Biol.* **2000**, *303*, 617−626.

(24) Bernad, S.; Oellerich, S.; Soulimane, T.; Noinville, S.; Baron, M. H.; Paternostre, M.; Lecomte, S. *Biophys. J.* **2004**, *86*, 3863−3872.

(25) Akiyama, S.; Takahashi, S.; Kimura, T.; Ishimori, K.; Morishima, I.; Nishikawa, Y.; Fujisawa, T. *Proc. Natl. Acad. Sci. U.S.A.* **2002**, *99*, 1329−1334.

(26) Rytomaa, M.; Kinnunen, P. K. J. *J. Biol. Chem.* **1995**, *270*, 3197−3202.

(27) Kawai, C.; Prado, F. M.; Nunes, G. L. C.; Di Mascio, P.; Carmona-Ribeiro, A. M.; Nantes, I. L. *J. Biol. Chem.* **2005**, *280*, 34709−34717.

(28) Rusu, L.; Gambhir, A.; McLaughlin, S.; Radler, J. *Biophys. J.* **2004**, *87*, 1044−1053.

(29) Trusova, V. M.; Gorbenko, G. P.; Molotkovsky, J. G.; Kinnunen, P. K. J. *Biophys. J.* **2010**, *99*, 1754−1763.

(30) Abdiche, Y.; Malashock, D.; Pinkerton, A.; Pons, J. *Anal. Biochem.* **2008**, *377*, 209−217.

(31) Domanov, Y. A.; Molotkovsky, J. G.; Gorbenko, G. P. *Biochim. Biophys. Acta, Biomembr.* **2005**, *1716*, 49−58.

(32) Nawrocki, J. P.; Chu, R.-A.; Pannell, L. K.; Bai, Y. *J. Mol. Biol.* **1999**, *293*, 991−995.

(33) Oellerich, S.; Lecomte, S.; Paternostre, M.; Heimburg, T.; Hildebrandt, P. *J. Phys. Chem. B* **2004**, *108*, 3871−3878.

(34) Pinheiro, T. J. T.; Cheng, H.; Seeholzer, S. H.; Roder, H. *J. Mol. Biol.* **2000**, *303*, 617−626. Jemmerson, R.; Liu, J.; Hausauer, D.; Lam, K. P.; Mondino, A.; Nelson, R. D. *Biochemistry* **1999**, *38*, 3599−3609. Bertini, I.; Turano, P.; Vasos, P. R.; Bondon, A.; Chevance, S.; Simonneaux, G. *J. Mol. Biol.* **2004**, *336*, 489−496.

(35) Belikova, N. A.; Vladimirov, Y. A.; Osipov, A. N.; Kapralov, A. A.; Tyurin, V. A.; Potapovich, M. V.; Basova, L. V.; Peterson, J.; Kurnikov, I. V.; Kagan, V. E. *Biochemistry* **2006**, *45*, 4998−5009.

(36) Balakrishnan, G.; Hu, Y.; Oyerinde, O. F.; Su, J.; Groves, J. T.; Spiro, T. G. *J. Am. Chem. Soc.* **2007**, *129*, 504−505. Diederix, R. E.; Ubbink, M.; Canters, G. W. *Biochemistry* **2002**, *41*, 13067−13077.

(37) Werner, J. H.; Joggerst, R.; Dyer, R. B.; Goodwin, P. M. *Proc. Natl. Acad. Sci. U.S.A.* **2006**, *103*, 11130−11135.

(38) Shastry, M. C. R.; Roder, H. *Nat. Struct. Biol.* **1998**, *5*, 385−392.

(39) Pascher, T.; Chesick, J. P.; Winkler, J. R.; Gray, H. B. *Science* **1996**, *271*, 1558−1560. Rischel, C.; Jorgensen, L. E.; Foldes-Papp, Z. *J. Phys.: Condens. Matter* **2003**, *15*, S1725−S1735.

(40) Pletneva, E. V.; Gray, H. B.; Winkler, J. R. *J. Am. Chem. Soc.* **2005**, *127*, 15370−15371.

(41) Heimburg, T.; Marsh, D. *Biophys. J.* **1995**, *68*, 536−546.

(42) Kostrzewa, A.; Pali, T.; Froncisz, W.; Marsh, D. *Biochemistry* **2000**, *39*, 6066−6074.

(43) Mileykovskaya, E.; Dowhan, W.; Birke, R. L.; Zheng, D.; Lutterodt, L.; Haines, T. H. *FEBS Lett.* **2001**, *507*, 187−190.

(44) Oellerich, S.; Lecomte, S.; Paternostre, M.; Heimburg, T.; Hildebrandt, P. *J. Phys. Chem. B* **2004**, *108*, 3871−3878. Rajagopal, B. S.; Silkstone, G. G.; Nicholls, P.; Wilson, M. T.; Worrall, J. A. R. *Biochim. Biophys. Acta, Bioenerg.* **2012**, *1817*, 780−791.

(45) Kalanxhi, E.; Wallace, C. J. *Biochem. J.* **2007**, *407*, 179−187.

(46) Rytömaa, M.; Kinnunen, P. K. *J. Biol. Chem.* **1994**, *269*, 1770−1774.

(47) Weinkam, P.; Pletneva, E. V.; Gray, H. B.; Winkler, J. R.; Wolynes, P. G. *Proc. Natl. Acad. Sci. U.S.A.* **2009**, *106*, 1796−1801.

(48) Ardail, D.; Privat, J. P.; Egret-Charlier, M.; Levrat, C.; Lerme, F.; Louisot, P. *J. Biol. Chem.* **1990**, *265*, 18797−18802. Schlame, M.; Rua, D.; Greenberg, M. L. *Prog. Lipid Res.* **2000**, *39*, 257−288.

(49) Garcia Fernandez, M.; Troiano, L.; Moretti, L.; Nasi, M.; Pinti, M.; Salvioli, S.; Dobrucki, J.; Cossarizza, A. *Cell Growth Differ.* **2002**, *13*, 449−455.

(50) Winkler, J. R. *Curr. Opin. Chem. Biol.* **2004**, *8*, 169−174. Bandi, S.; Bowler, B. E. *J. Am. Chem. Soc.* **2008**, *130*, 7540−7541.

(51) Maity, H.; Maity, M.; Englander, S. W. *J. Mol. Biol.* **2004**, *343*, 223−233.

(52) Hammack, B. N.; Smith, C. R.; Bowler, B. E. *J. Mol. Biol.* **2001**, *311*, 1091−1104.

(53) Weinkam, P.; Zong, C.; Wolynes, P. G. *Proc. Natl. Acad. Sci. U.S.A.* **2005**, *102*, 12401−12406.